JPE 19-2-23

https://doi.org/10.6113/JPE.2019.19.2.580
ISSN(Print): 1598-2092 / ISSN(Online): 2093-4718

Performance Improvement Strategy for Parallel-operated Virtual Synchronous Generators in Microgrids

Hui Zhang*, Ruixue Zhang*, Kai Sun†, and Wei Feng**

*College of Automation and Information Engineering, Xi'an University of Technology, Xi'an, China
†,**State Key Lab. of Power Systems, Department of Electrical Engineering, Tsinghua University, Beijing, China

Abstract

The concept of virtual synchronous generators (VSGs) is a valuable means for improving the frequency stability of microgrids (MGs). However, a great virtual inertia in a VSG's controller may cause power oscillation, thereby deteriorating system stability. In this study, a small-signal model of an MG with two paralleled VSGs is established, and a control strategy for maintaining a constant inertial time with an increasing active-frequency droop coefficient (m) is proposed on the basis of a root locus analysis. The power oscillation is suppressed by adjusting virtual synchronous reactance, damping coefficient, and load frequency coefficient under the same inertial time constant. In addition, the dynamic load distribution is sensitive to the controller parameters, especially under the parallel operation of VSGs with different capacities. Therefore, an active power increment method is introduced to improve the precision of active power sharing in dynamic response. Simulation and experimental is used to verify the theoretical analysis findings.

Key words: Active-frequency droop coefficient, Power oscillation, Virtual synchronous generator (VSG), Virtual synchronous reactance

I. INTRODUCTION

Recently, the solar power as renewable energy source, have been connected with utility grids by using a current-controlled inverter, which result in an increasingly serious effect on utility grids. Consequently, researchers [1]-[6] have proposed a virtual synchronous generator (VSG) technology, which make the inverters have the same characteristics of synchronous generator. The VSG is a new and interesting means of large-scale distributed generation (DG) in connecting with utility grids.

A conventional droop controller, which simulates the droop characteristic of a synchronous generator, is often adopted by inverters to share the active and reactive power in islanded mode [7-10]. However, the system's frequency stability cannot be guaranteed because the equivalent inertia is often small. Thus, a VSG control strategy for islanding mode is presented by introducing the rotor motion equation of a synchronous generator, thereby enhancing the frequency stability of a common alternating current (AC) bus. An improved control strategy of synchronverters is proposed [11], [12]. The inverter and synchronous generator are mathematically equivalent, but no current loop exists in the controller of synchronverters. Thus, the power quality of a grid-connected current is easily affected. The current loop is introduced, and the control strategy for parallel-operated VSGs is investigated to enhance the power quality [13]. However, the design methodology for parallel-operated VSGs with different capacities is not considered. A synchronous generator emulation control strategy for a voltage source converter (VSC)-HVDC station [14] is designed, in which the desired frequency support to a low-inertia grid is provided by the VSC station with the proposed control strategy. The system stability cannot be guaranteed when numerous, varying loads are connected to a weak power system. Thus, the effects of suppressing frequency fluctuations by using a VSG have

Manuscript received Jul. 7, 2018; accepted Dec. 3, 2018
Recommended for publication by Associate Editor Kyo-Beum Lee.
†Corresponding Author: sun-kai@mail.tsinghua.edu.cn
Tel: +86-10-62796934, Tsinghua University
*College of Autom. Inform. Eng., Xi'an University of Technol., China
**State Key Lab. Power Syst., Dept. Electr. Eng., Tsinghua Univ., China

been investigated [15], [16]. However, few studies have focused on stability analysis. A VSG with adaptive inertia is considered [17], [18] such that great inertia is used during acceleration, and small inertia is utilized to increase the deceleration effect. The introduction of a VSG's virtual inertia improves the frequency stability of an AC bus. However, power oscillation is not considered when a VSG is connected to the common AC bus [19]. A small-signal model for a VSG is established [20]-[22], and the stability in grid-connected and islanded modes is analyzed. However, the parallel-operated mode has not been evaluated.

A great virtual inertia effectively suppresses AC bus frequency fluctuation under frequent load disturbance and increases power oscillation when the VSG is connected to the common AC bus. Hence, a conventional droop control method is presented [23] to suppress power oscillation by introducing differential negative feedback. However, this method seriously affects the stability of a common AC bus. A power system stabilizer (PSS) is adopted [24], [25] to enhance the transient stability of a standalone microgrid (MG) system, which can also suppress power oscillation. The introduction of PSS parameters adds complexity to the design of controller parameters. Virtual admittance is adopted [26] to reduce the control runaway capability when the measured current is affected by harmonic, transient, and measured noises, which suppresses the power oscillation. However, the selection of virtual admittance parameter is not designed. Therefore, a control strategy is investigated to suppress power oscillation without influencing the system's frequency stability. Moreover, the VSG's output frequency slowly fluctuates with the occurrence of load disturbances, which is different from conventional droop control, and the dynamic response of the active power allocation of paralleled VSGs is inaccurate when the frequency variations of two VSGs are different. The power oscillation is suppressed by optimizing the parameters of the virtual impedance of VSG in parallel-operated VSGs with same capacities [29]. But the parallel operation of VSG with different capacities will increase power oscillation and return circuit current. Therefore, other parameters J, D, and K_ω, of the parallel VSG with same capacity are analyzed, and two methods to suppress power oscillation are proposed in this paper. In addition, the parameter design method for parallel-operated VSGs with different capacities is investigated.

An improved control strategy of VSG is proposed in Section II. The causes of power oscillation due to large virtual inertia are analyzed in Section III, two conditions are proposed: 1) increasing the difference coefficient, the damping coefficient, and the virtual inertia with the same proportion and 2) increasing the virtual synchronous reactance in an appropriate range. The parameter design method for parallel-operated VSGs with different capacities is investigated in Section IV. The effectiveness of the proposed method is verified through simulation and experiment in Sections V and VI, respectively, and the conclusions are presented in Section VII.

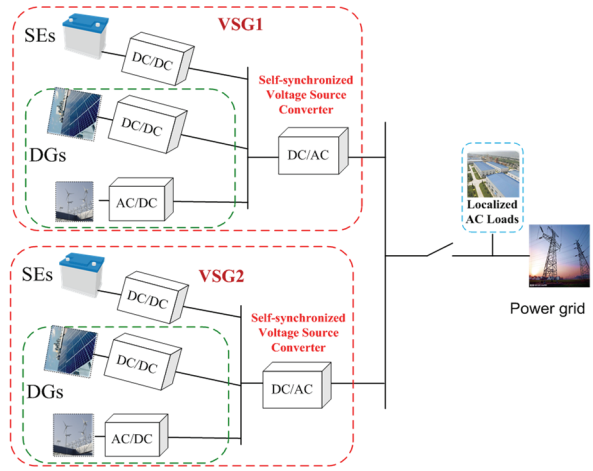

Fig. 1. Typical configuration of a VSG-based MG.

II. Design of a Self-Synchronized VSC

Fig. 1 shows a typical AC MG, in which the DGs and storage elements (SEs) are connected in parallel via the DC bus and then connected to the AC buses via self-synchronized VSCs. The VSG is constituted by DGs, SEs, and self-synchronized VSCs. For convenience, VSGs and self-synchronized VSCs are not distinguished in this study. VSGs often work in parallel to increase the capacity of an MG. Therefore, the analysis and discussion in this study focus on parallel-operated VSGs.

Fig. 2 shows the control block diagram of VSGs. The VSG control strategy consists of active power frequency, virtual synchronous reactance, and voltage/current control loops. u_{abc} is the output voltage of a VSG, u_{gabc} denotes the voltage of the AC bus, i_{abc} indicates the output current, and i_{Labc} represents the inductor current. The VSG contains a parallel pre-synchronization unit based on PLL to connect the AC bus.

A. Active Power Frequency Control

The active power frequency control of a VSG is reflected in the equations of prime-mover regulation and rotor motion [19]. The rotor motion is expressed as

$$\begin{cases} J\dfrac{\mathrm{d}\omega}{\mathrm{d}t} = T_m - T_e - D\Delta\omega = \dfrac{P_m}{\omega} - \dfrac{P_e}{\omega} - D(\omega - \omega_N) \\ \dfrac{\mathrm{d}\delta}{\mathrm{d}t} = \omega - \omega_N \end{cases}, \tag{1}$$

$$P_m = P_{ref} + K_\omega(\omega_{ref} - \omega), \tag{2}$$

where ω is the rotor angular velocity (rad/s), ω_{ref} represents the reference rotor angular velocity (rad/s), ω_N refers to the rated rotor angular velocity (rad/s), T_m stands for the mechanical torque (N·m), T_e indicates the electromagnetic torque (N·m), P_{ref} denotes the reference power (W), P_m signifies the mechanical power (W), P_e is the electromagnetic power (W), D represents the damping coefficient, J denotes the virtual inertia (kg·m^2), K_ω indicates the load frequency coefficient, and δ refers to the power angle (rad).

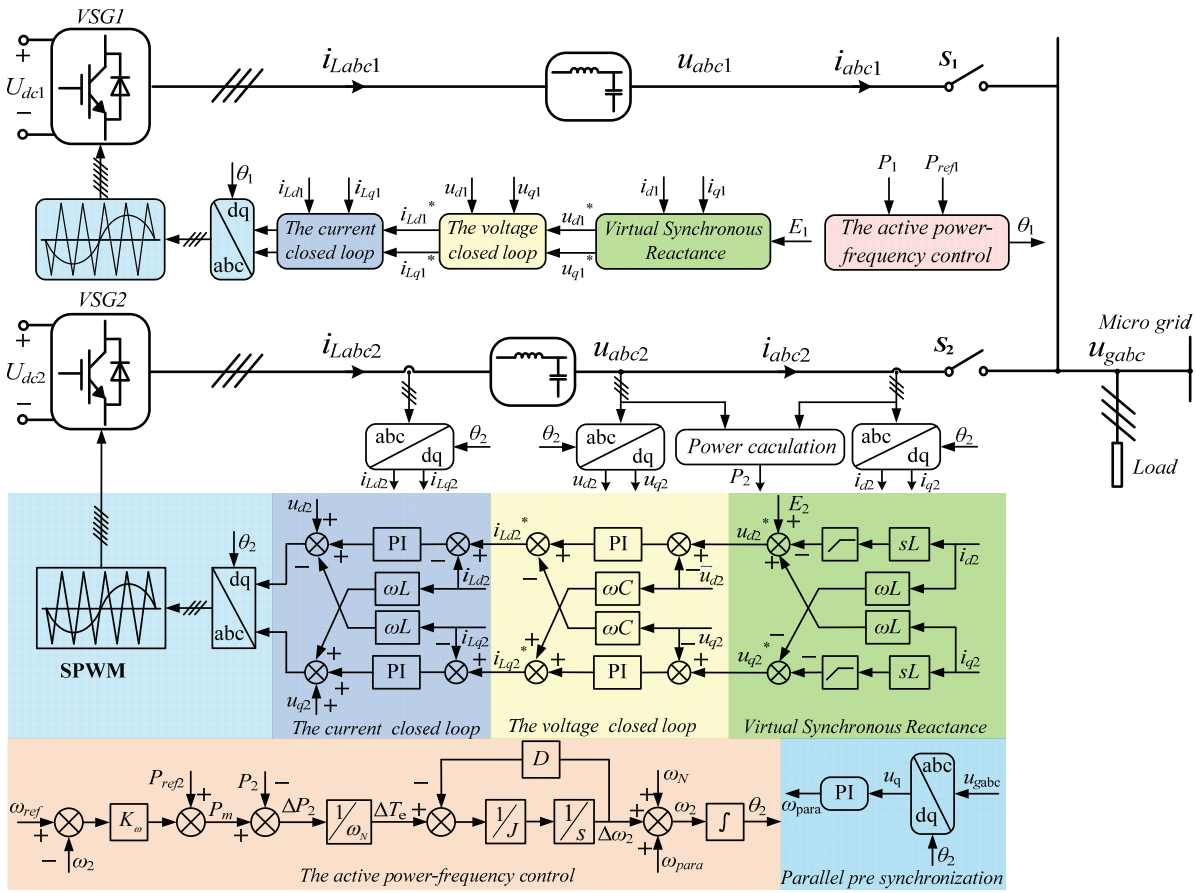

Fig. 2. Control block diagram of the VSG parallel system.

In the case of a small excursion of angular speed, ω can be represented by ω_N. Hence, Equation 1 can be changed to

$$\begin{cases} J\dfrac{\mathrm{d}\omega}{\mathrm{d}t} \approx T_m - T_e - D\Delta\omega = \dfrac{P_m}{\omega_N} - \dfrac{P_e}{\omega_N} - D(\omega - \omega_N) \\ \dfrac{\mathrm{d}\delta}{\mathrm{d}t} = \omega - \omega_N \end{cases} . \tag{3}$$

Therefore, the relationship between the frequency and output active power of a VSG by using Equations 2 and 3 can be written as

$$\frac{\omega_{ref} - \omega}{P_{ref} - P} = -\frac{1}{J\omega_N s + (D\omega_N + K_\omega)} = -\frac{m}{\tau s + 1}, \tag{4}$$

where

$$\begin{cases} \tau = \dfrac{J\omega_N}{D\omega_N + K_\omega} \\ m = \dfrac{1}{D\omega_N + K_\omega} \end{cases} .$$

B. Virtual Synchronous Reactance

The virtual synchronous reactance of a VSG is formed by synchronous generator's basic equation, as shown in Equation 5, which simulates the electrical part of the generator:

$$\begin{cases} u_d^* = -Ri_d + L\dfrac{di_d}{dt} + \omega L i_q + E \\ u_q^* = -Ri_q + L\dfrac{di_q}{dt} - \omega L i_d \end{cases} , \tag{5}$$

where u_d^* and u_q^* are the output voltage reference values in the dq frame; i_d and i_q represent the direct and quadrature output currents, respectively; and L and R denote the virtual synchronous reactance (H) and resistance (Ω), respectively. However, R is set to zero so that the VSG's equivalent output impedance indicates induction.

A VSG has a reactive power voltage droop characteristic due to the existence of virtual synchronous reactance in the controller. Therefore, VSGs can realize reactive power sharing. On the basis of power flow calculation and by ignoring the virtual reactive power loss via virtual synchronous reactance, the relationship between voltage amplitude U and reactive power Q can be calculated as

$$U = E - \frac{\omega L}{E} Q . \tag{6}$$

The VSG is suitable for hierarchical distribution networks due to virtual synchronous reactance L, and the output voltage and reactive power of VSG have a droop relationship. Besides,

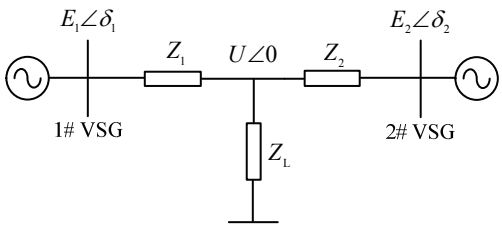

Fig. 3. Equivalent circuit of two-VSG systems.

the output reactive power can reduce AC bus voltage drop by removing the reactive power voltage droop control loop from the traditional droop control. Thus, the voltage quality can be improved compared with a conventional droop controller.

III. Suppression of Power Oscillation for Parallel-operated VSGs

The small-signal model is established to analyze the power oscillation of two paralleled VSGs based on MGs, as shown in Fig. 3. $E_1\angle\delta_1$ and $E_2\angle\delta_2$ are the output voltages of VSG1 and VSG2, respectively, and $U\angle 0$ represents the AC bus voltage. As the line impedance is ignored in the analysis, Z_1 and Z_2 stand for the equivalent output impedances of VSG1 and VSG2, respectively, and the load is Z_L.

The active power and angular frequency with small disturbance are calculated as

$$\begin{cases} \omega = \omega_s + \Delta\omega \\ P_e = P_{es} + \Delta P \end{cases}, \tag{7}$$

where ω_s and P_e are at the steady-state operating point and $\Delta\omega$ indicate the small disturbances of the VSG output frequency and ΔP denotes the small disturbances of the VSG active power. Therefore, the state equation can be derived from Equations 2, 3, and 4 as follows:

$$\begin{cases} \dfrac{d\Delta\delta_1}{dt} = \Delta\omega_1 \\ \dfrac{d\Delta\delta_2}{dt} = \Delta\omega_2 \\ \dfrac{d\Delta\omega_1}{dt} = -(\dfrac{K_{\omega 1}}{J_1\omega_N} + \dfrac{D_1}{J_1})\Delta\omega_1 - \dfrac{\Delta P_{e1}}{J_1\omega_N} \\ \dfrac{d\Delta\omega_2}{dt} = -(\dfrac{K_{\omega 2}}{J_2\omega_N} + \dfrac{D_2}{J_2})\Delta\omega_2 - \dfrac{\Delta P_{e2}}{J_2\omega_N} \end{cases}, \tag{8}$$

where $\Delta\delta_i$ refers to the power angle increment of each VSG. Then, the virtual electromagnetic power of the inverter can be calculated as

$$\begin{cases} \Delta P_{e1} = S_{E1}\Delta\delta_{12} \\ \Delta P_{e2} = S_{E2}\Delta\delta_{12} \end{cases}, \tag{9}$$

where

$$\begin{cases} S_{E1} = E_1E_2(-|G_{12}|\sin\delta_{12} + |B_{12}|\cos\delta_{12}) \\ S_{E2} = E_1E_2(-|G_{12}|\sin\delta_{12} - |B_{12}|\cos\delta_{12}) \end{cases}, \tag{10}$$

δ_{12} is the phase difference between VSG1 and VSG2, $\delta_{12} = \delta_1 - \delta_2$, and G_{12} and B_{12} denote the conductance and susceptance between VSG1 and VSG2, respectively.

Therefore, the small-signal state-space model of two paralleled VSGs can be derived from Equations 7, 8, and 9 as

$$\begin{pmatrix} \dfrac{d\Delta\delta_{12}}{dt} \\ \dfrac{d\Delta\omega_1}{dt} \\ \dfrac{d\Delta\omega_2}{dt} \end{pmatrix} = \begin{pmatrix} 0 & 1 & -1 \\ -\dfrac{S_{E1}}{J_1\omega_N} & -(\dfrac{K_{\omega 1}}{J_1\omega_N} + \dfrac{D_1}{J_1}) & 0 \\ -\dfrac{S_{E2}}{J_2\omega_N} & 0 & -(\dfrac{K_{\omega 2}}{J_2\omega_N} + \dfrac{D_2}{J_2}) \end{pmatrix} \begin{pmatrix} \Delta\delta_{12} \\ \Delta\omega_1 \\ \Delta\omega_2 \end{pmatrix}. \tag{11}$$

Therefore, the characteristic equation can be obtained as

$$s^3 + As^2 + Bs + C = 0, \tag{12}$$

where

$$A = \frac{K_{\omega 1}}{J_1\omega_N} + \frac{D_1}{J_1} + \frac{K_{\omega 2}}{J_2\omega_N} + \frac{D_2}{J_2}$$

$$B = \frac{K_{\omega 1}K_{\omega 2}}{J_1J_2\omega_N^2} + \frac{D_2K_{\omega 1}}{J_1J_2\omega_N} + \frac{D_1K_{\omega 2}}{J_1J_2\omega_N} + \frac{D_1D_2}{J_1J_2} + \frac{S_{E1}}{J_1\omega_N} - \frac{S_{E2}}{J_2\omega_N}$$

$$C = \frac{1}{J_1J_2\omega_N^2}(K_{\omega 2}S_{E1} - K_{\omega 1}S_{E2} + D_2\omega_N S_{E1} - D_1\omega_N S_{E2}).$$

Suppose that the same control parameters are adopted by VSG1 and VSG2. Then, the variables in Equation 12 can be simplified as follows:

$$A' = 2(\frac{K_\omega}{J\omega_0} + \frac{D}{J})$$

$$B' = \frac{K_\omega^2}{J^2\omega_0^2} + \frac{2DK_\omega}{J^2\omega_0} + \frac{D^2}{J^2} + \frac{1}{J\omega_0}(S_{E1} - S_{E2})$$

$$C' = \frac{1}{J^2\omega_0^2}[(K_\omega + D\omega_0)(S_{E1} - S_{E2})].$$

On the basis of Equations 4 and 12, the characteristic equation of the small-signal model can be reorganized as follows:

$$s^3 + \frac{2}{\tau}s^2 + \left[\frac{1}{\tau^2} + \frac{m}{\tau}(S_{E1} - S_{E2})\right]s + \frac{m}{\tau^2}(S_{E1} - S_{E2}) = 0. \tag{13}$$

As shown in Fig. 4, the equivalent impedance between two VSGs can be calculated as

$$Z_{12} = \frac{Z_1Z_2 + Z_1Z_L + Z_2Z_L}{Z_L} = R_{12} + jX_{12}, \tag{14}$$

where R_{12} and X_{12} are the resistive and inductive components of impedance, respectively.

The load capacity and control parameters of two VSGs are identical. Therefore, hypothetically, $\delta_{12} \approx 0$, and load impedance Z_L is set to 1 Ω. Furthermore, the relationship between S_{E1} and S_{E2} can be derived from Equation 10 to obtain

$$S_{E1} - S_{E2} = \frac{4E_1E_2}{\omega^3L^3 + 4\omega L}. \tag{15}$$

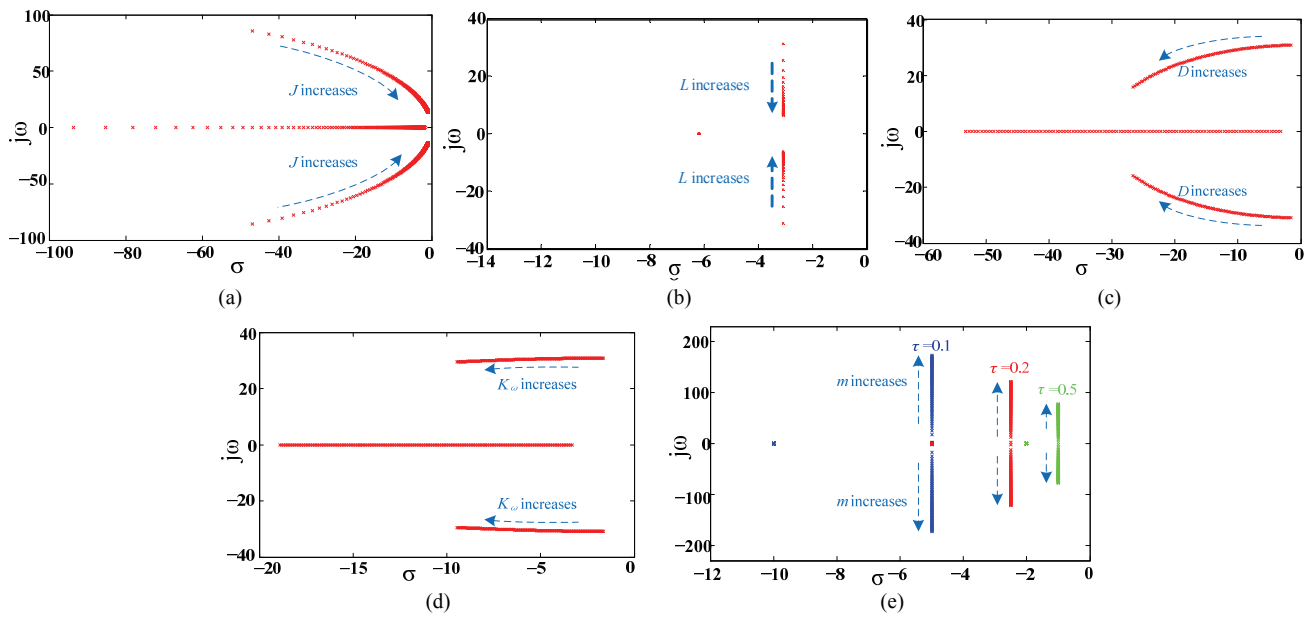

Fig. 4. Poles and zeros of: (a) $D = 3$, $K_\omega = 1{,}000$, $L = 1$ mH, $J = 0.1$ to 5. (b) $D = 3$, $J = 1$, $L = 0.1$ to 50 mH, $K_\omega = 1{,}000$. (c) $J = 1$, $L = 1$ mH, $K_\omega = 1{,}000$, $D = 0$ to 50. (d) $D = 3$, $J = 1$, $L = 1$ mH, $K_\omega = 10$ to 3,000. (e) $L = 1$ mH, $m = 0.000001$ to 0.01.

Then, the item of $S_{E1} - S_{E2}$ in the characteristic equation can be replaced.

Fig. 4 presents the root locus analysis of the model. As shown in Fig. 4(a), the dominant pole becomes close to the imaginary axis, and the system becomes unstable with the increase in virtual inertia J. However, the dominant pole moves toward the real axis with large virtual synchronous reactance L, which indicates that the system oscillation is suppressed, as shown in Fig. 4(b). Similarly, the system becomes stable with the increase in D and K_ω, as shown in Figs. 4(c) and (d), respectively. However, the dominant pole moves away from the real axis when the droop coefficient m increases and the system inertia time constant is unchanged, which indicates that the system damping is deteriorated. Moreover, when increasing inertial time constant τ, the dominant pole will move toward the imaginary axis, and the stability margin of the system is decreased, as shown in Fig. 4(e).

Therefore, two control strategies to suppress power oscillation are presented on the basis of the analysis:

(1) The inertial time should be kept constant with the increase of active frequency droop coefficient m, that is, D, J, and K_ω should be enhanced with the same scale.

(2) Increasing virtual synchronous reactance L.

IV. Parallel-Operated VSGs with Different Capacities

Fig. 2 shows the principle of the proposed control strategy. Generated real power P and reactive power Q are [27], [28] as follows:

$$P_i = \frac{E_i U}{Z_i} \sin \delta_i \,, \tag{16}$$

$$Q_i = \frac{E_i U}{Z_i} (\cos \delta_i - U) \,, \tag{17}$$

where i = 1, 2.

In this study, $E_1 = E_2 = E$, and the line impedance is not considered. Therefore, $Z_i = \omega L_i$, and the output active power of two VSGs is shown as follows

$$P_i = \frac{EU}{\omega L_i} \sin \delta_i \,. \tag{18}$$

With the increase in resistive load, the voltage drop caused by virtual impedance can be ignored compared with that caused by the reactive power on virtual synchronous reactance. The active power can be calculated as

$$P_i + \Delta P_i = \frac{EU}{\omega L_i} \sin(\delta_i + \Delta \delta_i) \,. \tag{19}$$

Generally, δ is less than 30° for a synchronous generator based on Equations 16, 18, and 19. In this case, sin δ ≈ δ and cos δ ≈ 1. Thus, the dynamic active power of two VSGs can be calculated as

$$\Delta P_i = \frac{EU}{\omega L_i} \sin(\delta_i + \Delta \delta_i) - \frac{EU}{\omega L_i} \sin(\delta_i) = \frac{EU}{\omega L_i} \sin \Delta \delta_i \tag{20}$$

where ΔP_i (i = 1, 2) represent the dynamic active power for VSG1 and VSG2, respectively, and $\Delta \delta_i$ (i = 1, 2) are the power angle variations. The load capacity ratio of VSG1 and VSG2 is set to C_1: C_2.

Sin Δδ can be simplified to Δδ because the power angle change is often relatively small. Therefore, we can rearrange Equation 20 as

$$\Delta P_i = \frac{EU}{\omega L_i} \Delta \delta_i \,. \tag{21}$$

The active power disturbance capacity ratio must remain constant when the load disturbance occurs to guarantee the active power sharing in the dynamic response, which is expressed as follows:

$$\frac{\Delta P_1}{\Delta P_2} = \frac{C_1}{C_2}. \tag{22}$$

Assuming that the resistive load increases at t_0 and the time span in which the frequency of the common AC bus changes to steady-state is Δt, the power angle increment of two VSGs can be calculated as

$$\Delta\delta_i = \int_{t_0}^{t_0+\Delta t} \Delta\omega_i dt. \tag{23}$$

Considering that $P_{ref} = 0$, Equation 24 can be derived by combining Equations 4, 21, 22, and 23, which is expressed as follows:

$$\frac{\Delta\omega_1(s)}{\Delta\omega_2(s)} = \frac{E_1X_2}{E_2X_1}\frac{J_1\omega_N s + (D_1\omega_N + K_{\omega 1})}{J_2\omega_N s + (D_2\omega_N + K_{\omega 2})} = \frac{C_1}{C_2}. \tag{24}$$

The active power disturbance capacity ratio of VSGs in the dynamic response remains constant. The control parameters of two VSGs are determined on the basis of the following:

$$\frac{L_2}{L_1} = \frac{J_1}{J_2} = \frac{D_1}{D_2} = \frac{K_{\omega 1}}{K_{\omega 2}} = \frac{C_1}{C_2}. \tag{25}$$

On the basis of Equations 6 and 17, the output reactive power of two VSGs when the inductive load increases can be calculated as

$$Q_i = \frac{E\left(U - \frac{\omega L_i}{E}\Delta Q_i\right)}{\omega L_i}\left[\cos\delta - \left(U - \frac{\omega L_i}{E}\Delta Q_i\right)\right], \tag{26}$$

where ΔQ_i (i = 1, 2) are the dynamic reactive power values for VSG1 and VSG2, respectively.

Therefore, dynamic reactive power ΔQ_i based on Equations 17 and 26 can be calculated as

$$\Delta Q_i = (2U - \cos\delta - 1)\frac{E}{\omega L_i}. \tag{27}$$

Considering that the reactive power disturbance capacity ratio must be kept constant when load disturbance occurs, we have

$$\frac{\Delta Q_1}{\Delta Q_2} = \frac{C_1}{C_2}. \tag{28}$$

The reactive power disturbance capacity ratio of VSGs in the dynamic response remains constant based on Equations 27 and 28, and the control parameters of two VSGs can be calculated as

$$\frac{L_2}{L_1} = \frac{C_1}{C_2}. \tag{29}$$

On the basis of Equations 25 and 29 designed parameters of VSGs with different capacities, the dynamic response of active and reactive power allocated by capacity can be improved.

TABLE I
PARAMETERS OF SIMULATIONS

	Symbols	Parameters
DC bus voltage (V)	U_{dci}	200
Filter inductors (mH)	L_{fi}	2
Filter capacitor (uF)	C_{fi}	50
Switching frequency (Hz)	f	5,000
Reference frequency (rad/s)	ω_{ref}	314
No-load voltage (V)	E_d	80
DC capacitor (uF)	C	3300

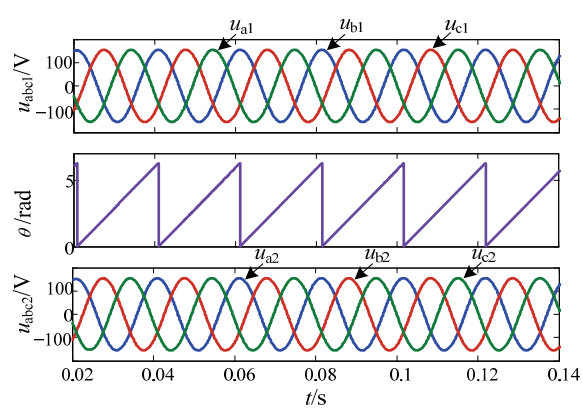

Fig. 5. Simulation waveform for VSG output voltage and AC bus voltage.

V. SIMULATION RESULT

To verify the accuracy of the proposed control and improved parameter design methodology, a simulation model of two paralleled VSGs is established in MATLAB/Simulink. Table I lists the parameters of the controller and power stage.

A. Simulation for Pre-synchronization

The phase of the VSG must be the same as that of the AC bus before the VSG is connected to the AC bus, and the pre-synchronization for parallel-operated VSGs must be determined. Fig. 5 shows the simulated voltage waveforms of a VSG and AC bus. The voltage phase of the VSG can be synchronized to the AC bus by using a pre-synchronization method.

B. Simulation for Power Oscillation Suppression

As shown in Fig. 6, VSG1 normally operates with a resistive load of approximately 400 W in the beginning, and VSG2 is switched at 1.0 s. Active power oscillation remarkably increases with the increase in virtual inertia *J* when the VSG is connected to the AC bus by keeping all other parameters unchanged. This condition is consistent with the small-signal analysis, Fig. 4(a) shows that large virtual inertia affects the stability of the VSG parallel system.

Fig. 7 shows the same scenario is used to determine the power damping influence of droop coefficient *m*. The overshoot and oscillation of the output active power are effectively suppressed with a large damping coefficient and virtual inertia when the

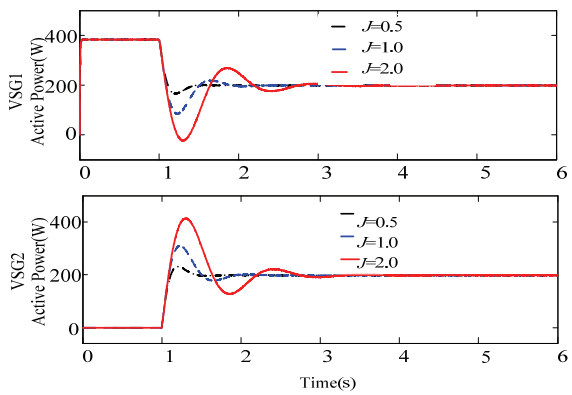

Fig. 6. Simulation waveforms for active power with different J values.

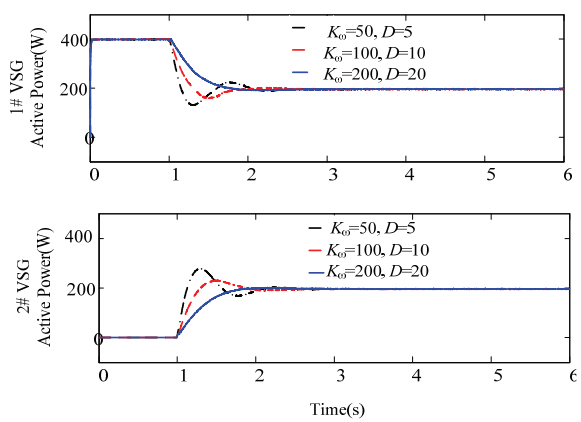

Fig. 7. Simulation waveforms for active power with different m values.

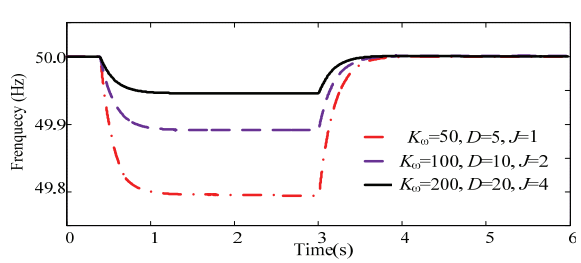

Fig. 8. Simulation waveforms for AC bus frequency with different parameters.

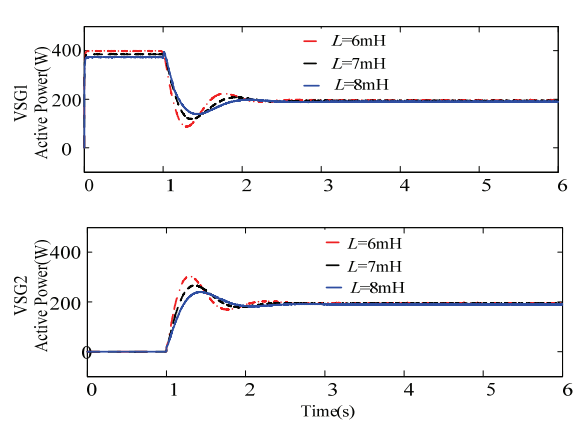

Fig. 9. Simulation waveforms for active power with different L values.

TABLE II
PARAMETERS OF SIMULATIONS

Parameter	VSG1		VSG2	
	Optimized	Not optimized	Optimized	Not optimized
D	5	5	3	3
J	2	2	1.2	2
K_ω	50	50	30	30
L	0.006	0.006	0.01	0.01

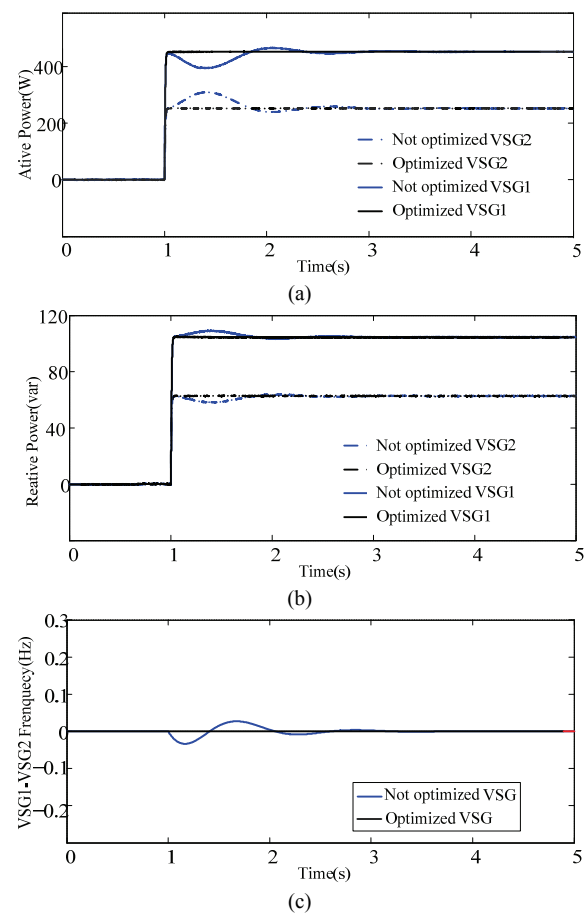

Fig. 10. Simulation waveforms of the VSG parallel system with different load capacities. (a) Active power of parallel-operated VSGs. (b) Reactive power of parallel-operated VSGs. (c) Frequency of parallel-operated VSGs.

damping coefficient, virtual inertia, and load frequency coefficient are accordingly adjusted with the same time constant τ. This finding is consistent with the results of small-signal analysis, as shown in Fig. 4(e). System damping is enhanced, and the oscillation is suppressed with large values of J, D, and K_ω.

As shown in Fig. 8, the time of frequency curve recovery to steady state is unchanged with the increase of J, D, and K_ω, which is approximately 1.0 s. The stability of frequency is not affected.

The same scenario is used to evaluate the power damping influence of virtual synchronous reactance L, as shown in Fig. 9. Active power fluctuation is smoothed and suppressed with

large values of L. This condition is consistent with the results of small-signal analysis. As shown in Fig. 4(b), system damping is enhanced, and the oscillation is suppressed with large values of L.

C. Simulation for Parallel-operated VSGs with Different Capacities

Simulation: Parallel-operated VSGs with resistive loads operate, resistive and inductive loads are added at 1.5 s, and the load capacity ratio is set to C_1:C_2 = 5:3. Table II lists the simulation parameters.

As shown in Fig. 10(a), the active power sharing performance is improved after the optimization of parameters. The system is moved to stable operation point within 0.1 s, whereas the original system takes approximately 2.5 s. Moreover, the dynamic reactive power sharing performance is improved, as exhibited in Fig. 10(b). As presented in Fig. 10(c), the relative frequency difference between VSG1 and VSG2 is not zero due to the non-optimized parameters in 1–3 s.

VI. Experimental Results

In order to verify the effectiveness of the control strategy, an experimental platform was developed, which includes two VSGs, an LC filter, a DSP control board, and a resistive load, as shown in Fig. 11. Table III lists the parameters of the power stage.

A. Contrast Experiment for Traditional Droop and VSG Controls

The experimental waveforms of the VSG and AC bus is shown as Fig. 12. The voltage of the VSG can be synchronized to the AC bus through pre-synchronization.

B. Power Oscillation Suppression for Parallel-operated VSGs

Figs. 13 and 14 present the operation waveforms of VSGs with different values of J, D, and K_ω. These waveforms are obtained by using a D/A converter. As shown in Figs. 13(a), (b), and (c), a large active power oscillation occurs in the parallel system when VSG2 is connected to the AC bus with small J, D, and K_ω values. However, the output active power of VSGs becomes smooth with the increase of J, D, and K_ω. The inertia time is kept constant. Figs. 14(a), (b), and (c) show the frequency waveforms of the AC bus. The parameters are consistent with Figs. 13(a), (b), and (c), in which the active load increases and active power decreases. In addition, the time of frequency curve recovery to steady state is unchanged with the increase of J, D, and K_ω at the same rate, which is approximately 1 s. Hence, the frequency stability of the AC bus is unchanged. Thus, the increase of J, D, and K_ω at the same rate can decrease the power oscillation and overshoot, and improve the parallel system's stability.

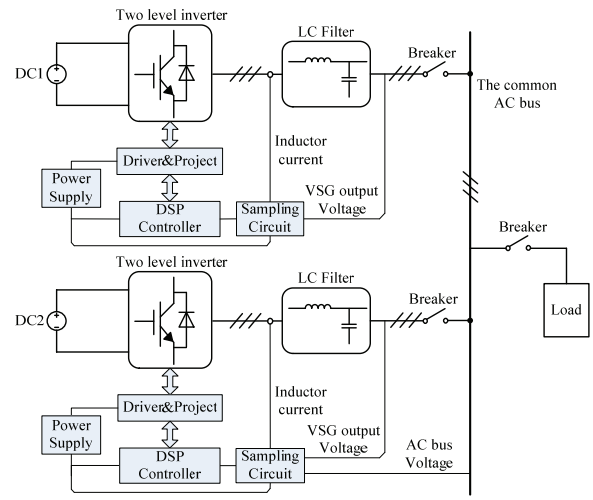

(a)

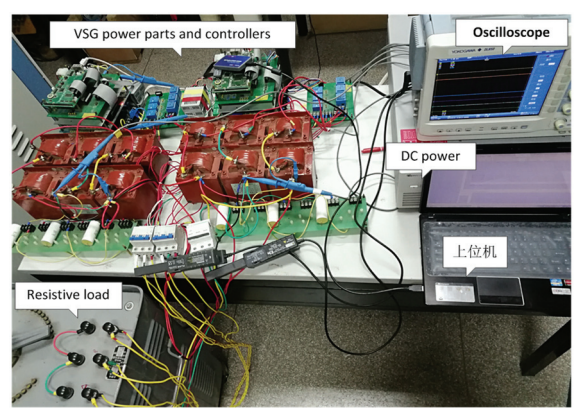

(b)

Fig. 11. Experimental platform of parallel-operated VSGs. (a) Schematic of the experimental setup. (b) Photo of the experimental platform.

TABLE III
Parameters of Experiments

	Symbols	Parameters
DC bus voltage (V)	U_{dci}	200
Filter inductors (mH)	L_{fi}	2
Filter capacitor (uF)	C_{fi}	50
Switching frequency (Hz)	f	5,000
No-load frequency (rad/s)	ω_0	314
No-load voltage (V)	E	80

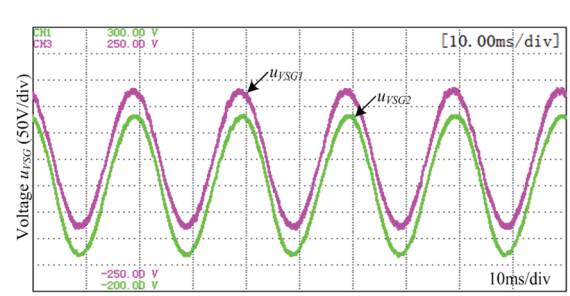

Fig. 12. Experimental waveform of the output voltage of VSG and AC bus voltage.

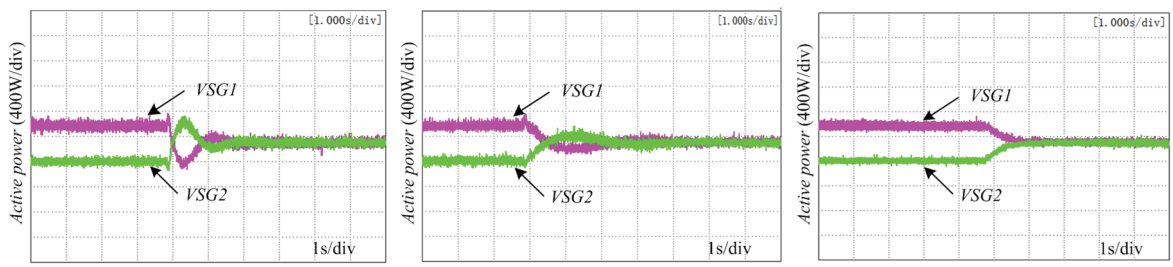

(a) (b) (c)

Fig. 13. Output active power experimental waveforms of VSG parallel system. (a) $D = 2$, $J = 0.5$, $K_\omega = 100$, $L = 0.006$. (b) $D = 3$, $J = 0.75$, $K_\omega = 150$, $L = 0.006$. (c) $D = 4$, $J = 1$, $K_\omega = 200$, $L = 0.006$.

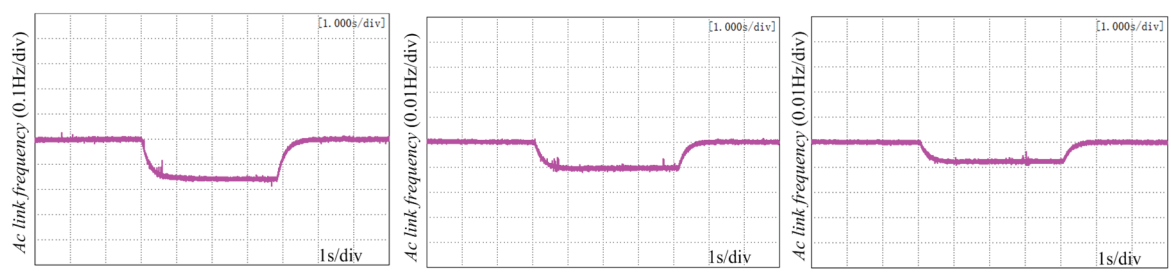

(a) (b) (c)

Fig. 14. Frequency waveforms of the AC bus .(a) $D = 2$, $J = 0.5$, $K_\omega = 100$, $L = 0.006$. (b) $D = 3$, $J = 0.75$, $K_\omega = 150$, $L = 0.006$. (c) $D = 4$, $J = 1$, $K_\omega = 200$, $L = 0.006$.

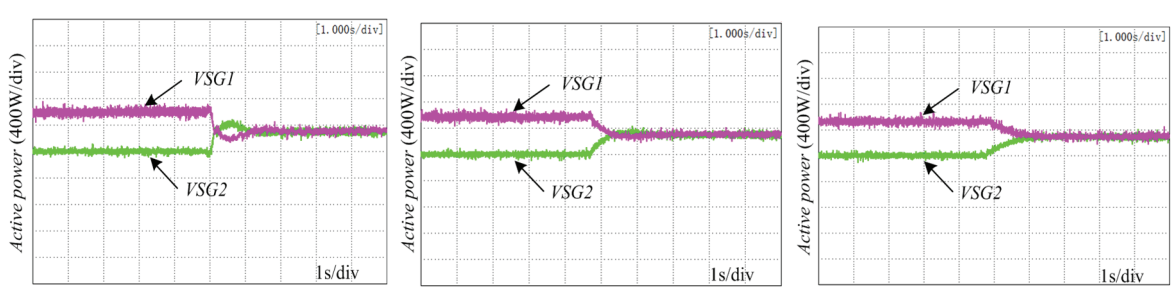

(a) (b) (c)

Fig. 15. Output active power experimental waveforms of VSG parallel system. (a) $D = 3$, $J = 0.6$, $K_\omega = 150$, $L = 0.005$. (b) $D = 3$, $J = 0.6$, $K_\omega = 150$, $L = 0.008$. (c) $D = 3$, $J = 0.6$, $K_\omega = 150$, $L = 0.01$.

Fig. 15 exhibits the operation waveforms of VSGs with different values of L. A large power oscillation occurs in the parallel system when VSG2 is connected to the AC bus with a small virtual synchronous reactance. However, the output active power of VSGs becomes smooth with the increase of virtual synchronous reactance. Thus, the increase of L can reduce the overshoot, suppress the power oscillation, and improve the parallel system's stability. The increase of L is effective for suppressing power oscillations.

C. Parallel-operated VSGs with Different Capacities

The design methodology of parallel-operated VSGs with different capacities is verified by experiment. Table IV lists the controller parameters.

Fig. 16(a) presents the experimental waveforms of load step disturbance without optimized parameters. The current amplitude of VSG1 slowly increases. However, the VSG2 current slowly decreases, and the output currents of the two VSGs' dynamic current distributions are not proportional to the load capacity ratio.

TABLE IV
OPTIMIZED SYSTEM PARAMETERS FOR THE EXPERIMENT

Parameter	VSG1		VSG2	
	Optimized	Not optimized	Optimized	Not optimized
D	5	5	3	3
J	2	2	1.2	2
K_ω	50	50	30	30
L	0.006	0.006	0.01	0.01

Fig. 16(b) shows the experimental waveforms of load step disturbance with optimized parameters. The dynamic currents of the two VSGs meet the load capacity ratio when a disturbance occurs, which is consistent with the simulation results. The experimental results verify the effectiveness of the designed parameters for parallel-operated VSGs with different capacities.

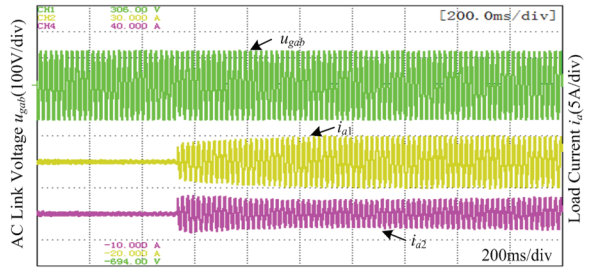

(a)

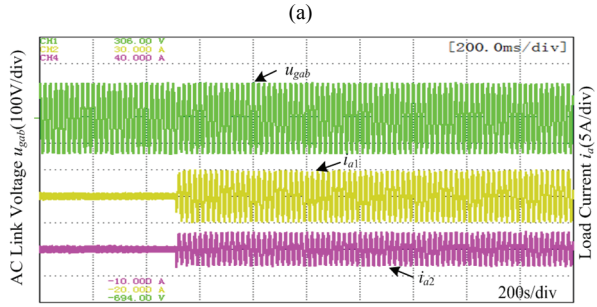

(b)

Fig. 16. Experimental waveforms of VSG parallel system with different load capacities. (a) Parameters are not optimized. (b) Parameters are optimized.

VII. Conclusion

This study investigates the mechanism of power oscillation in parallel-operated VSGs on the basis of a small signal model, and an improved control strategy is presented without altering inertia time constant to suppress power oscillation: 1) The inertial time should be kept constant with the increase of active frequency droop coefficient m, that is, D, J, and K_ω should be enhanced with the same scale; 2) Increasing virtual synchronous reactance L. The simulation and experiment results verify the effectiveness of the proposed control strategy. The frequency stability of the common AC bus is improved, and power oscillations are suppressed. Moreover, the dynamic power sharing precision is effectively enhanced by using an improved parameter design method for parallel-operated VSGs with different capacities.

Acknowledgment

This paper is sponsored by the National Natural Science Foundation of China (51877175, 61733010, and 51677054); Key Research Program of Shaanxi Province (2017ZDXM-GY-003); and Xi'an Science and Technology Plan (2017080CG/RC043).

References

[1] H.-P. Beck and R. Hesse, "Virtual synchronous machine," in *Proceedings of the 9th International Conference on Electrical Power Quality and Utilisation*, pp. 1-6, 2007.

[2] F. Gao and M. R. Iravani, "A control strategy for a distributed generation unit in grid-connected and autonomous modes of operation," *IEEE Trans. Power Del.*, Vol. 23, No. 2, pp. 850-859, Apr. 2008.

[3] J. Alipoor, Y. Miura, and T. Ise, "Distributed generation grid integration using virtual synchronous generator with adoptive virtual inertia," *2013 IEEE Energy Conversion Congress and Exposition*, pp. 4546-4552, 2013.

[4] T. Shintai, Y. Miura, and T. Ise, "Oscillation damping of a distributed generator using a virtual synchronous generator," *IEEE Trans. Power Del.*, Vol. 29, No. 2, pp. 668-676, Apr. 2014.

[5] J. Alipoor, Y. Miura, and T. Ise, "Power system stabilization using virtual synchronous generator with alternating moment of inertia," *IEEE J. Emerg. Sel. Topics Power Electron.*, Vol. 3, No. 2, pp. 451-458, Jun. 2015.

[6] Q. C. Zhong and G. Weiss, "Static synchronous generators for distributed generation and renewable energy," P*ower Systems Conference and Exposition, 2009. PSCE '09. IEEE/PES*, pp. 1-6, 2009.

[7] M. John, P. A. Mendoza-Araya, and G. Venkataramanan, "Small signal impedance measurement in droop controlled AC microgrids," *2014 IEEE Energy Conversion Congress and Exposition (ECCE)*, pp. 702-709, 2014.

[8] J. C. Vasquez, J. M. Guerrero, M. Savaghebi, and R. Teodorescu, "Modeling, analysis, and design of stationary reference frame droop controlled parallel three-phase voltage source inverters," *Power Electronics and ECCE Asia (ICPE & ECCE), 2011 IEEE 8th International Conference on*, pp. 272-279, 2011.

[9] J. C. Vasquez, J. M. Guerrero, M. Savaghebi, J. Eloy-Garcia, and R. Teodorescu, "Modeling, analysis, and design of stationary-reference-frame droop-controlled parallel three-phase voltage source inverters," *IEEE Trans. Ind. Electron.*, Vol. 60, No. 4, pp. 1271-1280, Apr. 2013.

[10] T. Wu, Z. Liu, J. Liu, S. Wang, and Z. You, "A unified virtual power decoupling method for droop-controlled parallel inverters in microgrids," *IEEE Trans. Power Electron.,* Vol. 31, No. 8, pp. 5587-5603, Aug, 2016.

[11] Q. C. Zhong and G. Weiss, "Synchronverters: Inverters that mimic synchronous generators," *IEEE Trans. Ind. Electron.*, Vol. 58, No. 4, pp. 1259-1267, Apr. 2011.

[12] Q. C. Zhong, P. L. Nguyen, Z. Ma, and W. Sheng, "Self-synchronized synchronverters: inverters without a dedicated synchronization unit," *IEEE Trans. Power Electron.*, Vol. 29, No. 2, pp. 617-630, Feb. 2014.

[13] C. Cheng, Z. Zeng, H. Yang, and R. Zhao, "Wireless parallel control of three-phase inverters based on virtual synchronous generator theory," *Electrical Machines and Systems (ICEMS), 2013 International Conference on*, pp. 162-166, 2013.

[14] M. Guan, W. Pan, J. Zhang, Q. Hao, J. Cheng, and X. Zheng, "Synchronous generator emulation control strategy for voltage source converter (VSC) stations," *IEEE Trans. Power Syst*, Vol. 30, No. 6, pp. 3093-3101, Nov. 2015.

[15] Y. Hirase, O. Noro, K. Sugimoto, K. Sakimoto, Y. Shindo, and T. Ise, "Effects of suppressing frequency fluctuations by parallel operation of virtual synchronous generator in microgrids," *2015 IEEE Energy Conversion Congress and Exposition (ECCE)*, pp. 3694-3701, 2015.

[16] Y. Hirase, O. Noro, K. Sugimoto, K. Sakimoto, Y. Shindo, and T. I. Osaka, "Effects and analysis of suppressing frequency fluctuations in microgrids using virtual synchronous generator control," *Industrial Electronics Society, IECON 2015 - 41st Annual Conference of the IEEE*, pp. 43-49, 2015.

[17] J. Alipoor, Y. Miura, and T. Ise, "Distributed generation grid integration using virtual synchronous generator with

adoptive virtual inertia," *2013 IEEE Energy Conversion Congress and Exposition*, pp. 4546-4552, 2013.

[18] J. Alipoor, Y. Miura, and T. Ise, "Power system stabilization using virtual synchronous generator with alternating moment of inertia," *IEEE J. Emerg. Sel. Topics Power Electron.*, Vol. 3, No. 2, pp. 451-458, Jun. 2015.

[19] Y. Du, J. Su, M. Mao, and X. Yang, "Autonomous controller based on synchronous generator dq0 model for micro grid inverters," *IEEE ECCE Asia,* pp. 2645-2649, 2011.

[20] J. Liu, Y. Miura, and T. Ise, "Comparison of dynamic characteristics between virtual synchronous generator and droop control in inverter-based distributed generators," *IEEE Trans. Power Electron.*, Vol. 31, No. 5, pp. 3600-3611, May 2016.

[21] J. Liu, Y. Miura, and T. Ise, "Dynamic characteristics and stability comparisons between virtual synchronous generator and droop control in inverter-based distributed generators," *2014 International Power Electronics Conference (IPEC-Hiroshima 2014 - ECCE ASIA)*, pp. 1536-1543, 2014.

[22] H. Wu, X. Ruan, D. Yang, X. Chen, W. Zhao, Z. Lv, and Q.-C. Zhong, "Small-signal modeling and parameters design for virtual synchronous generators," *IEEE Trans. Ind. Electron.*, Vol. 63, No. 7, pp. 4292-4303, Jul. 2016.

[23] J. M. Guerrero, L. G. de Vicuna, J. Matas, M. Castilla, and J. Miret, "A wireless controller to enhance dynamic performance of parallel inverters in distributed generation systems," *IEEE Trans. Power Electron.,* Vol. 19, No. 5, pp. 1205-1213, Sep. 2004.

[24] R. M. Santos Filho, P. F. Seixas, P. C. Cortizo, G. Gateau, and E. A. A. Coelho, "Power system stabilizer for comunicationless parallel connected inverters," *2010 IEEE International Symposium on Industrial Electronics*, pp. 1004-1009, 2010.

[25] W. A. Habri and Y. L. A. Magid, "Power system stabilizer for power distribution control of parallel inverters in a grid –Connected micro-grid system," *Innovative Smart Grid Technologies-Middle East (ISGT Middle East), 2011 IEEE PES Conference on*, pp. 1-8, 2011.

[26] P. Rodriguez, C. Citro, I. Candela, J. Rocabert, and P. Rodriguez, "Flexible grid connection and islanding of SPC-based PV power converters," *IEEE Trans. Ind. Appl.* Vol. 54, No. 3, pp. 2690–2702, May/Jun. 2018.

[27] T. Wildi, *Electrical Machines, Drives and Power Systems*, 6th ed. EnglewoodCliffs, NJ, USA: Prentice-Hall, 2005.B.

[28] B. Singh, R. Saha, A. Chandra, and K. Al-Haddad, "Static synchronous compensators (STATCOM): A review," *IET Power Electron.*, Vol. 2, No. 4, pp. 297-324, Jul, 2009.

[29] Y. Wei, H. Zhang, Q. Song, and K. Sun, "Control strategy for parallel-operated virtual synchronous generators," *2016 International Power Electronics and Motion Control Conference (IPEMC-ECCE Asia 2016),* pp. 2015-2021, 2016.

Hui Zhang received B.S., M.S., and Ph.D. degrees in electrical engineering from HUST, Wuhan, China, in 1985, 1990, and 2002, respectively. He was as a post-doctoral researcher in XAUT and Yongji Electric Machine Factory of CNR Corporation from 2003 to 2005. He served as a senior visiting scholar at Tsinghua University, PRC, from 2007 to 2008 and a senior visiting professor at VT, USA, from 2010 to 2011. He is currently a professora Ph.D. supervisor, and academic leader of power electronics and power drives at XAUT. His research interests include MG control, energy storage control, wheel-driven electric vehicles, electric traction, and electric propulsion.

Ruixue Zhang received a B.E. degree in electrical engineering and automation from Luoyang Normal University, Luoyang, China, in 2015. She received her master's degree from Xi'an University of Technology in 2015 and majored in electrical engineering. At present, she is studying at Tsinghua University as a joint training student. Her current research interests include VSG and grid-connected inverters.

Kai Sun received B.E., M.E., and Ph.D. degrees in electrical engineering from Tsinghua University, Beijing, China, in 2000, 2002, and 2006, respectively. He joined the faculty of Electrical Engineering, Tsinghua University, in 2006, where he is currently an associate professor. From Sep 2009 to Aug 2010, he served as a visiting scholar at the Department of Energy Technology, Aalborg University, Aalborg, Denmark. From Jan to Aug 2017, he served as a visiting professor at the Department of Electrical and Computer Engineering, University of Alberta, Edmonton, Canada. His current research interests include power electronics for renewable generation systems, microgrids, and energy internet. Dr. Sun is a member of the IEEE Power Electronics Society Sustainable Energy Systems Technical Committee, IEEE Power Electronics Society Power and Control Core Technologies Committee, and IEEE Industrial Electronics Society Renewable Energy Systems Technical Committee. Dr. Sun serves as an associate editor for *IEEE Transactions on Power Electronics, IEEE Journal of Emerging and Selected Topics in Power Electronics*, and *Journal of Power Electronics*. Dr. Sun served as the TPC vice chair of IEEE ECCE2017 and IEEE ECCE-Asia 2017. He also served as the general co-chair of the 2018 International Future Energy Challenge (IFEC2018). He was a recipient of Delta Young Scholar Award in 2013 and Youth Award of China Power Supply Society in 2017.

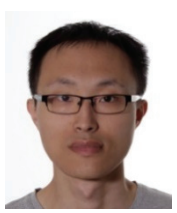

Wei Feng received B.S. and M.S. degrees in automation from the Beijing Jiaotong University, Beijing, China, in 2006 and 2008, respectively. He received a Ph.D. degree in power electronics and motor drive from the Institute of Electrical Engineering, Chinese Academy of Sciences, Beijing, in 2014. He is currently a post-doc in Tsinghua University, China. His research interests include control of paralleled inverters for renewable generation systems, power quality improvement, and energy management system for MGs.